3D-printed high-resolution microchannels for contrast enhanced ultrasound research

Roger Domingo-Roca
Department of Biomedical Engineering
University of Strathclyde
Glasgow, United Kingdom
roger.domingo-roca@strath.ac.uk

Lauren Gilmour
Department of Biomedical Engineering
University of Strathclyde
Glasgow, United Kingdom
lauren.gilmour@strath.ac.uk

Lisa Asciak
Department of Biomedical Engineering
University of Strathclyde
Glasgow, United Kingdom
lisa.asciak@strath.ac.uk

Stylianos Sarrigiannidis
James Watt School of Engineering
University of Glasgow
Glasgow, United Kingdom
stylianos.sarrigiannidis@gla.ac.uk

Oana Dobre
James Watt School of Engineering
University of Glasgow
Glasgow, United Kingdom
oana.dobre@gla.ac.uk

Manuel Salmeron-Sanchez
James Watt School of Engineering
University of Glasgow
Glasgow, United Kingdom
manuel.salmeron-sanchez@gla.ac.uk

Mairi Sandison
Department of Biomedical Engineering
University of Strathclyde
Glasgow, United Kingdom
mairi.sandison@strath.ac.uk

Richard O'Leary
Electronic and Electrical Engineering
University of Strathclyde
Glasgow, United Kingdom
richard.oleary@strath.ac.uk

Joseph Jackson-Camargo
Electronic and Electrical Engineering
University of Strathclyde
Glasgow, United Kingdom
joseph.jackson@strath.ac.uk

Helen Mulvana
Department of Biomedical Engineering
University of Strathclyde
Glasgow, United Kingdom
helen.mulvana@strath.ac.uk

***Abstract*—Systemically circulating microbubbles are used as contrast agents to aid both drug targeting and delivery using ultrasound. Exploiting their acoustic behaviour in small diameter vessels is critical for both applications, but the highly controlled experiments required to support this are not possible *in vivo* and challenging *in vitro*. Experimental platforms with small diameter channels (below 200 microns) are not readily available nor able to represent vascular geometries, leaving the existence and extent of microbubble-microvessel interactions incompletely defined. In this work we present a 3D-printed microchannel platform using tissue-mimicking hydrogels featuring radii down to 75 microns. We demonstrate application to study microbubble behaviour via acoustic backscatter under controlled environments in physiologically-relevant conditions.**

Keywords—Microbubbles, ultrasound contrast agents, backscatter, microvessels, 3D-printing.

I. INTRODUCTION

Intravenously injected microbubbles (MBs) in the blood pool can be excited by ultrasound to enhance contrast in ultrasound imaging. When this happens, MBs undergo linear and non-linear oscillations and backscatter sound waves [1]. These backscattered echoes generate characteristic signatures that have been exploited to improve contrast in ultrasound imaging [2-5]. This is possible due to the non-linear content of the backscattered signal, as the sound scattered by MBs in the blood pool can be separated from that scattered by the surrounding tissue to image perfusion. Ultrasound-driven MBs have also been used to disrupt the blood brain barrier [6] and promote the uptake of chemotherapy treatments by exerting local forces on nearby cellular surfaces to enhance porosity [6]. In each application, MB oscillations influence the nature and frequency content of the backscattered ultrasound signal, offering consequent opportunity for exploitation. In imaging, this may allow information relating to the local conditions experienced by the MB to be recovered, for example proximity to the blood vessel wall or blood flow rate. In therapy, application opportunities may exist to improve closed loop control processes.

The response of MBs to an acoustic field depends on a number of factors, such as the frequency of excitation, MB size, and shell properties [7,8]. In general, for low amplitude excitation, MBs undergo oscillation that can generally be approximated to be linear, around the equilibrium radius of the MB. As the driving amplitude increases, oscillations become increasingly non-linear in nature, with the consequent generation of harmonics of the fundamental driving frequency (f_0) [8,9]. While non-linear propagation of ultrasound waves in tissue can also lead to the evolution of harmonics [10,11], the generation of sub-harmonic ($f_0/2$) and ultra-harmonic ($nf_0/2$, with n = 3, 5, 7,) emissions are exclusive signatures of MB activity [8,12-14], and can therefore be used to faithfully determine its existence. However, there exists other biological phenomena capable of influencing MB behaviour and therefore the properties of the backscattered sound. These can include blood flow velocity and MB proximity to the wall, where the influence of each on MB behaviour has been relatively less studied. Mathematical models have been developed to describe the influence of some of these parameters on isolated MBs [5,15-18], but some of them use rigid boundary conditions, which are irrelevant for clinical translation. Approaches *in vitro* don't use physiologically-relevant platforms, focus on single MBs, or study biophysical factors that do not provide information about MB behaviour [3,4,18,19]. *In vivo* studies, additionally, use samples which physiology cannot be controlled, hindering systematic study of sets of parameters on MB behaviour [2,20]. Therapeutic applications of ultrasound to treat cancer have been widely

investigated [21-23] as the re-radiated acoustic pressure could air targeting cell permeability through sonoporation, leading to better therapeutic outcomes [25, 26]. The existence of micro-vessel flow phantoms that can be applied within ultrasound research will support detailed investigation of these phenomena within controlled environments. The emerging outcomes may be used to develop a better understanding of MB signatures under ultrasound excitation.

In this paper we report the use of a 3D-printed platform for ultrasound research developed in our lab. The flow phantoms present physiologically-relevant features using tissue-mimicking materials. We discuss how this can be used to investigate MB backscatter signatures under a given set of ultrasound excitation and physiologically-relevant conditions, e.g. mechanical index (MI), and flow rate (Q).

II. Materials and Methods

A. *Preparation of hydrogel resin and 3D-printing calibration*

Bisphenol-A ethoxylate dimethacrylate (BEMA, 1.7 kDa, Sigma Aldrich) hydrogel (20 wt%) were prepared by dissolving the polymer in de-ionised water. After polymer dissolution under constant stirring, 39 mM of lithium phenyl-2,4,6-trimethylbenzoylphosphinate (LAP, Sigma Aldrich) was added to the aqueous solution. When LAP was totally dissolved, 8.63 mM of tartrazine were added to the solution. The mixture was stirred for 30 minutes before translation to the 3D printer (Pico2HD27UV, ASIGA). LAP is a Type-I photoinitiator that, when exposed to UV light (λ_{abs} = 375 nm [27]), links to the methacrylate groups present in BEMA, leading to full networking of the hydrogel through radical chain polymerisation. Tartrazine is a synthetic photoblocker with strong absorbance at 405 nm and that does not bind to the hydrogel and has therefore the ability to diffuse (up to a 70%, [28]), leading to transparent hydrogels.

The resin was placed in the 3D printer vat and was optically calibrated by removing the build block and exposing the liquid resin to the 385 nm wavelength light at a set of energies (from 498 mJ/cm^2 to 998 mJ/cm^2). Each of the energies within this set generated a solid rectangular film. These films were removed from the vat, measured, and plotted vs the provided energy values. The resulting plot was fitted using the Beer-Lambert law, which provides the characteristic parameters of the resin. The second step of the calibration process consists of determining the amount of microchannel occlusion generated in the 3D-printing process by evaluating the amount of over-curing generated by the layers that are 3D-printed below the micro-channels. This was done by 3D-printing a set of 5 square microchannels (500x500 µm cross section) placed at different heights, from 100 µm to 900 µm in steps of 200 µm (layer thickness, l_z, 10 µm).

B. *Acoustic characterisation of 3D-printed hydrogels*

Acoustic measurements were performed to determine the speed of sound. A block of hydrogel was 3D-printed (30x30x5 mm) as a test object. In anticipation of the speed of sound being approximately that of water, 2.25 MHz (Olympus, A304S-SU, f = 2.25 MHz) was chosen to ensure that the material to test was several wavelengths thick. The transducer was driven by a pulser-receiver (WaveMaker, Marco Design Ltd.) in pulse-echo mode, and the output connected to an oscilloscope (Tektronix, DPO4054B). To test the material, the hydrogel sample (stored in water and thus in its fully-swollen state) was briefly removed from storage and placed directly on the transducer face. There was sufficient moisture remaining on the material to provide a full water coupling between transducer and sample. Time traces on the oscilloscope were used to calculate the time between successive echoes. We used the onset of the pulse as the timings for the first and second echo and calculated the speed of sound from the time difference between the first and second echo, and the distance travelled by the pulse. Time differences were measured both directly from the receive signal peaks and in addition by cross-correlation of the transmitted and received signals.

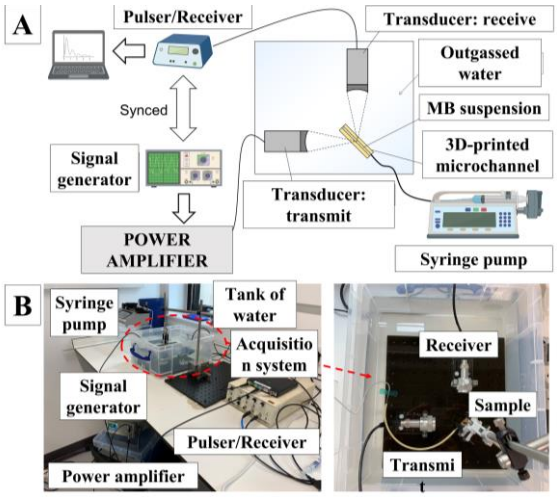

Fig. 1: (A) Schematic of experimental set up for acquiring MB backscattered signals. (B) Picture of the experimental set up.

C. *Measurement of the mechanical properties of the 3D-printed hydrogels*

The elastic modulus (E) of the hydrogel was determined by rheology and nanoindentation. Rheological measurements were carried out by using a stress-controlled rheometer (MCR, Anton Paar) equipped with a parallel plate geometry (upper plate diameter, 15 mm) at room temperature. Strain sweeps (0.01 – 1% range) and angular frequency (10 rad^{-1}) were performed to determine the elastic shear modulus.

Nanoindentation measurements were performed using a nano-indentation device (Chiaro, Optics11, Amsterdam, NL) mounted on top of an inverted phase contrast microscope (Evos XL Core, Thermofisher, Paisley, UK) using a spherical tip. Measurements were performed in 15x15 arrays at a speed of 2 µm/s over a vertical range of 10 µm. The selected cantilever had a stiffness of 32 mN/m and held a spherical tip of 8 µm in radius. The collected data was analysed using a custom software programmed in Python 3.0 (Python Software Foundation). The indentation depth was obtained from the penetration-load curves acquired from nanoindentation assays and the mechanical properties were calculated by fitting the experimental data using the Hertz model.

D. *Microbubble acoustic backscattering measurements.*

Acoustic backscatter signals were acquired from a matched pair of single-element transducers (f = 3.5 MHz, Panametrics) positioned at 90° from one another in a tank of outgassed water such that the micro-vessel contained within the flow phantom was located at the mutual focus. Flow was controlled using a syringe pump (0, 30, and 50 µL/min, LEGATO110) to reproduce different regimes of physiologically-relevant velocities, and 200 µL bolus of MBs

(SonoVue, Bracco) was added. The transmit transducer was driven at 3.5 MHz (10 cycles burst, PRF 10 ms) via signal generator (AFG3102, Tektronics) and amplifier (A300, E&I). Signals scattered by the micro-vessel/MBs were acquired as soon as the bolus reached the focal region of the backscatter set-up, acoustically identified from the signals observed on an oscilloscope. Backscattered signals were amplified (50 dB) and received via a pulser/receiver (PRF35, JSR) and acquired to a PC (Handyscope HS5, TiePie NL). The experiment was repeated across a range of MIs (0.10, 0.20, 0.30, 0.40, and 0.50) and Q (0, 30, and 50 µL/min), see Fig. 1.

III. Resuts and Discussion

A. Resin preparation and direct light processing

The thicknesses of the samples produced for calibration were measured (from 101 µm to 143 µm, using micro computed tomography) and used to determine the characteristic parameters of the resin using the Beer-Lambert law. The characteristic penetration depth, D_p, and critical energy, E_c, were determined to be, respectively (±s.e.), (58.36±1.43) µm and (87.06±0.25) mJ/cm^2. These parameters were used to determine that, at 10 µm layer thickness, channel occlusion increased by 1% every 20 layers, following $\sum_{n=0}^{N} E_0 e^{-nl_z/D_p} = \left(e^{-Nl_z/D_p} - A\right)/B$, where E_0 is the dose at the bottom of the vat, $A = e^{-l_z/D_p}$, $B = 1 - A$, and N is the number of layers 3D-printed below the channel. Determining these parameters enabled 3D-printing of high-resolution, physiologically-relevant microchannels.

B. Acoustic and mechanical properties

The speed of sound of the hydrogel was calculated to be of (±s.e.) (1394.59±0.17) m/s using cross-correlation. Point measurements of the pulse-echo response indicates that the speed of sound is between 1387.39 m/s and 1566.50 m/s. The density of the hydrogel was measured to be (±s.e.) (1110.78±20.20) kg/m^3. Young's modulus (E) was determined from stress-controlled rheology and nanoindentation, providing values of E (±s.e.) of (51.78±0.75) kPa, and (55.65±1.87) kPa, respectively. An ideal material for reconstructing tissue phantoms for biomedical research should have the same ranges of speeds of sound (1440 – 1600 m/s [29]) and attenuation coefficients (0.73 – 3.3 dB cm^{-1} MHz^{-1} [30]) which we have successfully demonstrated.

C. Acoustic backscattering

3D-printed tissue mimicking hydrogel micro-vessel flow systems were demonstrated for experimental investigation of MB backscatter signals, from which the characteristic harmonic peaks representative of MBs oscillation could be recovered (Fig. 2). After successful confirmation of MB activation in our experimental set up, we controlled Q and MI during MB flow through the microchannel to investigate its impact on the frequency content of the backscattered signal.

We observed that as flow rate increases the characteristic ultra-harmonics lose spectral energy, while f_0 harmonics tend to gain spectral energy and become more apparent. We measured f_0 harmonics in all experiments but as reported in previous studies, these are not necessarily an indication of MB activity as they can be generated by tissue (or by tissue-mimicking materials) as a consequence of the nonlinear propagation of ultrasound waves [10,11]. Hence, looking at spectral energy at the sub-harmonics and/or ultra-harmonics was determined to be a better indicator of MB activity, as these peaks cannot be generated by other components present

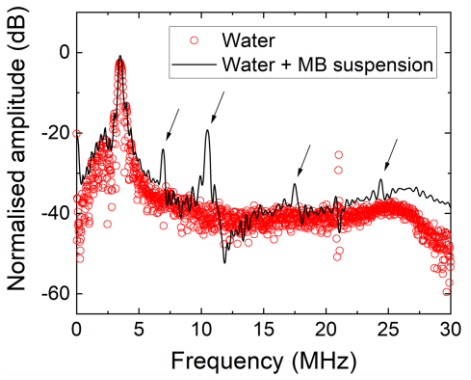

Fig. 2: The log frequency spectra of sound scattered from water-filled micro-vessels with and without suspended MBs under flow. Arrows indicate harmonics generated by MBs, not observed when MBs are not present.

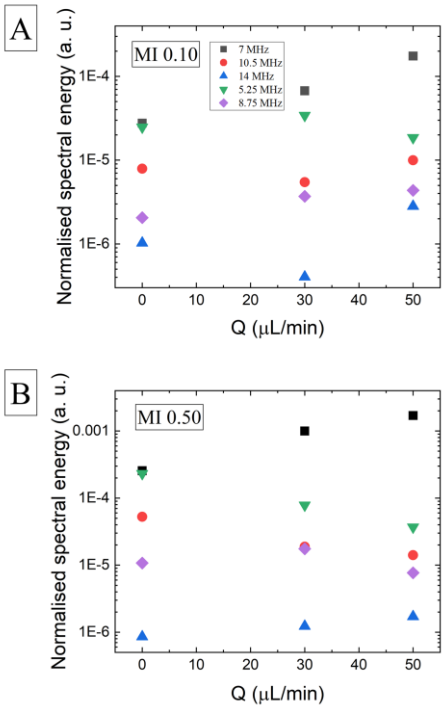

Fig. 3: (A) and (B) show the averaged normalised spectral energy of the measured peaks backscattered by flowing microbubbles at different flow rates, and mechanical indices of 0.10 and 0.50, respectively.

in the system. As expected, this effect becomes more apparent with increasing MI. As Q increases, the harmonic-to-ultra-harmonic ratio increases, with this effect becoming more apparent at higher MI values. We hypothesize that this may occur as a result of buoyancy effects as, at lower Q (MB velocity is slower, tending to 0 m/s, leading to estimated travel times of around 0.13 s for the MBs to get close to the wall), MBs will travel closer to the microchannel wall and change their modes of oscillation, leading to characteristic modes that do not appear when the MBs flow through the centre of the microchannel (as they will follow the streamlines of laminar flow within the microchannel). We observed that at lower Qs, more prominent ultra-harmonic peaks appeared, with higher amplitudes and thus carrying more spectral energy than some of the harmonics ($3f_0$ and $4f_0$). As Q values change the laminar flow profile within the micro-vessels, this will have direct consequences affecting the location where MBs travel within

the vessel. We hypothesize that the consequent broadening of the flow focus at low Q values will alter the spatial distribution of MBs in the vessel such that they will scatter ultrasound differently, producing characteristic signatures that will depend on the degree of MB-micro-vessel interaction. Though requiring further investigation, our hypothesis may be supported by the influence of vessel wall proximity on MB oscillation, where MBs located close to a wall oscillate non-symmetrically, leading to the generation of higher harmonics and ultra-harmonic content [8,12-17].

IV. Conclusions

We have demonstrated development of 3D-printable, photo-responsive, tissue-mimicking hydrogels that can be 3D-printed through direct light processing. These hydrogels present mechanical and acoustic properties similar to tissue and can be used to 3D-print high-resolution channels (down to 75 μm in radius) in physiologically-relevant morphologies. We have shown that such microchannels can be used to study how biologically-relevant parameters (flow rate, mechanical index) influence the ultrasound signal backscattered from circulating SonoVue microbubbles. Data gathered so far may indicate that MBs closer to the wall show marked differences in the spectral profile of their backscattered ultrasound signal, indicated by increased spectral energy at both higher (from $3f_0$) and ultra-harmonics. These preliminary findings require further investigation, which will be focus of our future work.

References

[1] M. Emmer, A. van Wamel, D. E. Goertz, and N. de Jong, "The onset of microbubble vibration", Ultrasound Med. Biol., vol. 33, pp. 941–949, November 2006.

[2] T. Faez, I. Skachkov, M. Versluis, K. Kooiman, and N. de Jong, "In vivo characterization of ultrasound contrast agents: microbubble spectroscopy in a chicken embryo", Ultrasound Med. Biol., vol. 38, pp. 1608-1617, May 2012.

[3] V. Garbin, D. Cojoc, E. Ferrari, and E. Di Fabrizio, "Changes in microbubble dynamics near a boundary revealed by combined optical micromanipulation and high-speed imaging", Appl. Phys. Lett., vol. 90, pp. 114103, February 2007.

[4] S. Zhao, D. E. Kruse, K. W. Ferrara, and P. A. Dayton, "Aocoustic response from adherent targeted contrast agents", JASA-EL, vol. 120, pp. 63-69, December 2006.

[5] S. Martynov, E. Stride, and N. Saffari, "The natural freqeuncy of microbubble oscillation in elastic vessels", J. Acoust. Soc. Am., vol. 126, pp. 2963-2972, December 2009.

[6] N. Hosseinkhah, D. E. Goertz, and K. Hynynen, "Microbubbles and blood brain barrier opening: a numerical study on acoustic emissions and wall stress predictions", IEEE Trans. Biomed. Eng., vol. 62, pp. 1293-1304, August 2015.

[7] C. Sun, V. Sboros, M. B. Butler, and C. M. Moran, "In vitro characterization of three phospholipid ultrasound contrast agents from 12 to 43 MHz", Ultrasound Med, Biol., vol. 40, pp. 541-550, October 2013.

[8] J. R. McLaughlan, S. Harput, R. H. Abou-Saleh, S. A. Peyman, S. Evans, and S. Freear, "Characterisation of liposome-loaded microbubble populations for subharmonic imaging", Ultrasound Med. Biol., vol. 43, pp. 346-356, September 2016.

[9] N. de Jong, A. Boukaz, and P. Frinking, "Basic acoustic properties of microbubbles", Ecochardiography, vol. 19, pp. 229-240, April 2002.

[10] M.-X. Tang, N. Kamiyama, and R. J. Eckersley, "Effects of onlinear propagation n ultrasound contrast agent imaging", Ultrasound Med. Biol.. vol. 36, pp. 459-466, November 2009.

[11] Y. O. Yildiz, R. J. Eckersley, R. Senior, A. K. P. Lim, D. Cosgrove, and M.-X. Tang, "Correction of non-linear propagation artifact in contrast-enhanced ultrasound imaging of carotid arteries: methods and in vitro evaluation", Ultrasound Med. Biol., vol. 41, pp. 1938-1947, March 2015.

[12] D. E. Goertz, M. E. Frijlink, and N. de Jong, "High frequency nonlinear scattering from a micrometer to submicrometer sized lipid encapsulated contrast agent", Ultrasound Med. Biol., vol. 32, pp. 569-577, January 2006.

[13] M. A. O'Reilly, K. Hynynen, "Blood-brain barrier: real-time feedback-controlled focused ultrasound disruption by using an acoustic emissions-based controller", Radiology, vol. 263, pp. 96-106, April 2012.

[14] G. Yanjun, Z. Dong, and G. Xiufen, "Subharmonic and ultraharmonic emissions based on the nonlinear oscillation of encapsulated microbubbles in ultrasound contrast agents", Sci. Bull., vol. 50, pp. 1975-1978, September 2005.

[15] A. A. Doinikov, L. Aired, and A. Bouakaz, "Dynamics of a contrast agent microbubble attached to an elastic wall", IEEE Trans. Med. Imaging, vol. 31, pp. 654-662, October 2011.

[16] J.-W. Hu, L.-M. Wang, S.-Y. Qian, W.-Y. Liu, Y.-T. Liu, and W.-R. Lei, "Dynamics of an ultrasound contrast agent microbubble near a spherical boundary in ultrasound field", Chin. Phys. B., vol. 28, 114301, October 2019.

[17] N. Mobadersany, and K. Sarkar, "Acoustic microstreaming near a plane wall due to a pulsating free or coated bubble: velocity, vorticity, and closed streamlines", J. Fluid. Mech., vol. 875, PP. 781-806, June 2019.

[18] E. K. Juang, I. De Cock, C. Keravnou, M. K. Gallagher, S. B. Keller, Y. Zheng, and M. Averkiou, "Engineered 3D microvascular networks for the study of ultrasound-microbubble-mediated drug delivery", Langmuir, vol. 35, pp. 10128-10138, December 2018.

[19] J. Deprez, G. Lajoinie, Y. Engelen, S. C. De Smedt, and I. Lentacker, "Opening doors with ultrasound and microbubbles: beating biological barriers to promote drug delivery", Adv. Drug. Deliv. Rev., vol. 172, pp. 9-36, March 2021.

[20] Y.-J. Ho, H.-C. Chang, C.-W. Lin, C.-H. Fan, Y.-C. Lin, K.-C. Wie, and C.-K. Yeh, "Oscillatory behavior of microbubbles impacts efficacy of cellular drug delivery", J. Control. Release, vol. 333, pp. 316-327, March 2021.

[21] A. L. Klibanov, and J. A. Hossack, "Ultrasound in radiology: from anatomic, funtional, molecular imaging to drug delivery and image-guided therapy", Invest Riol., vol. 50, pp. 657-670, September 2016.

[22] D. R. Mittelstein, J. Ye, E. F. Schibber, A. Roychoudhury, L. T. Martinez, M. H. Fekrazad, M. Ortiz, P. P. Lee, M. C. Shapiro, and M. Gharib, "Selective ablation of cancer cells with low intensity pulsed ultrasound", App. Phys. Lett., vol. 116, 013701.

[23] N. Ingram, et al., "Ultrasound-triggered therapeutic microbubbles enhance the efficacy of cytotoxic drugs by increasing circulation and tumor drug accumulation and limiting bioavailability and toxicity n normal tissues", Theranostics, vol. 10, pp. 10973-10992, September 2020.

[24] A. Delalande, S. Kotopoulis, and M. Postema, "Sonoporation: mechanistic insights and ongoing challenges for gene transfer", Gene, vol. 525, pp. 191-199, August 2013.

[25] K. Kooiman, H. J. Vos, M. Versluis, and N. de Jong, "Acoustic behaviuor of microbubbles and implications for drug delivery", Adv. Drug Deliv. Rev., vol. 72, pp. 28-48, June 2014.

[26] J. McLaughlan, N. Ingram, P. R. Smith, S. Harput, P. L. Coletta, S. Evans, and S. Freear, "Increasing the sonoporation efficiency of targeted polydisperse microbubble populations using chirp excitation", IEEE Trans. Ultrason. Ferroelectr. Freq. Control, vol. 60, pp. 2511-2520, December 2013.

[27] R. Domingo-Roca, B Saltin, J. F. C. Windmill, J. Jackson, H. Mulvana, "Rapid prototyped microvessel flow pahntom for controlled investigation of ultrasound-mediated targeted drug delivery", IEEE IUS, pp. 2390-2393, 2019.

[28] A. D. Benjamin, R. Abbasi, M. Owens, R. J. Olsen, D. J. Walsh, T. B LeFevre, and J. N. Wilking, "Light-based 3D printing of hydrogels with high-resolution channels", Biomed. Phys. Eng. Express, vol. 5, 025035, January 2019.

[29] E. L. Madsen, J. A. Zagzebski, R. A. Banjavie, and R. E. Jutila, "Tissue mimicking materials for ultrasound phantoms", Med. Phys., vol. 5, pp. 391-394, September 1978.

[30] A. Goldstein, and R. L. Powis, "Medical ultrasonic diagnosis", New York, NY, Academic Press, 1998..